



Photolytic fractionation of seven singly and doubly substituted nitrous oxide isotopocules measured by quantum cascade laser absorption spectroscopy

Journal Article

Author(s):

Kantnerova, Kristyna ; Jespersen, Malte F.; Bernasconi, Stefano M. ; Emmenegger, Lukas; Johnson, Matthew S.; Mohn, Joachim

Publication date:

2020-12

Permanent link:

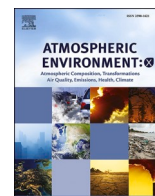
<https://doi.org/10.3929/ethz-b-000447393>

Rights / license:

Creative Commons Attribution-NonCommercial-NoDerivatives 4.0 International

Originally published in:

Atmospheric Environment: X 8, <https://doi.org/10.1016/j.aeaoa.2020.100094>



Photolytic fractionation of seven singly and doubly substituted nitrous oxide isotopocules measured by quantum cascade laser absorption spectroscopy

Kristýna Kantnerová^{a,b,1,*}, Malte F. Jespersen^{c,1}, Stefano M. Bernasconi^b, Lukas Emmenegger^a, Matthew S. Johnson^c, Joachim Mohn^a

^a Empa, Laboratory for Air Pollution / Environmental Technology, Dübendorf, 8600, Switzerland

^b ETH Zürich, Department of Earth Sciences, Zürich, 8092, Switzerland

^c University of Copenhagen, Department of Chemistry, Copenhagen, 2100, Denmark

ARTICLE INFO

Keywords:

UV photolysis
Nitrous oxide
Clumped isotopes
QCLAS

ABSTRACT

There is strong interest in using isotopic analysis to better constrain the budget of atmospheric nitrous oxide (N_2O). This interest is supported by emerging instruments that allow analysis of multiply substituted species. We have studied fractionation during UV photolysis of singly and doubly isotopically substituted molecules (isotopocules) of N_2O . N_2O was photolyzed in an electropolished stainless-steel reactor using a broadband laser-driven light source with bandpass filters. Isotopocule ratios were quantified at different stages of photolysis using a quantum cascade laser absorption spectroscopy (QCLAS) system. Wavelength-dependent fractionation constants were determined using the Rayleigh distillation model. The fractionation constants for photolysis with 200 nm and 214 nm bandpass filters, respectively, for the seven most abundant isotopocules of N_2O (after $^{14}\text{N}^{14}\text{N}^{16}\text{O}$) are: $^{14}\text{N}^{15}\text{N}^{16}\text{O}$ (456): $(-48.9 \pm 7.4) \text{‰} / (-82.4 \pm 22.3) \text{‰}$, $^{15}\text{N}^{14}\text{N}^{16}\text{O}$ (546): $(-22.2 \pm 5.3) \text{‰} / (-36.1 \pm 19.6) \text{‰}$, $^{14}\text{N}^{14}\text{N}^{17}\text{O}$ (447): $(-12.7 \pm 4.5) \text{‰} / (-21.9 \pm 15.7) \text{‰}$, $^{14}\text{N}^{14}\text{N}^{18}\text{O}$ (448): $(-33.5 \pm 12.0) \text{‰} / (-44.1 \pm 29.8) \text{‰}$, $^{14}\text{N}^{15}\text{N}^{18}\text{O}$ (458): $(-80.9 \pm 6.5) \text{‰} / (-120.9 \pm 23.7) \text{‰}$, $^{15}\text{N}^{14}\text{N}^{18}\text{O}$ (548): $(-52.7 \pm 10.8) \text{‰} / (-79.1 \pm 28.5) \text{‰}$, $^{15}\text{N}^{15}\text{N}^{16}\text{O}$ (556): $(-66.9 \pm 9.8) \text{‰} / (-110.9 \pm 27.5) \text{‰}$. The fractionation constants determined here for isotopocules 456, 546, 447, 448, and 556 are in agreement with previous theoretical models employed in this study and previous experiments. For 458 and 548, the fractionation constants were determined for the first time, confirming the prediction of more negative fractionation for ^{15}N substitution in the central position. The effect of stratospheric photolysis on the clumped isotope Δ values of tropospheric N_2O was found to be modest with $\Delta^{458} = (4.0 \pm 1.0) \text{‰}$, $\Delta^{548} = (-4.0 \pm 1.0) \text{‰}$, and $\Delta^{556} = (-1.5 \pm 1.0) \text{‰}$ at 9% photolysis. Therefore, atmospheric variations of doubly substituted N_2O isotopocules will likely be dominated by the characteristics of the N_2O sources, which strongly supports their value for source attribution and quantification.

1. Introduction

Nitrous oxide (N_2O) is a potent greenhouse gas with a global warming potential that is 300 times larger than that of CO_2 on a 100-year time scale (Griffis et al., 2017). In addition, N_2O is the most important anthropogenic ozone-depleting chemical of the twenty-first century (Ravishankara et al., 2009). The mole fraction of atmospheric N_2O has increased from $270 \text{ nmol mol}^{-1}$ in the pre-industrial era to

$331 \text{ nmol mol}^{-1}$ in 2018 (World Meteorological Organization and Global Atmosphere Watch, 2019). The increase is mainly driven by the rising use of agricultural fertilizer (Griffis et al., 2017; Syakila and Kroeze, 2011), which stimulates nitrification and denitrification, the two main microbial sources of N_2O (Toyoda et al., 2017).

There is significant uncertainty in the atmospheric N_2O budget as the biological sources are diffuse. In contrast to numerous N_2O sources, there are only few sink processes. The main atmospheric loss processes

* Corresponding author. Empa, Laboratory for Air Pollution / Environmental Technology, Dübendorf, 8600, Switzerland.

E-mail addresses: kantnerova.kristyna@gmail.com (K. Kantnerová), malte@chem.ku.dk (M.F. Jespersen), stefano.bernasconi@erdw.ethz.ch (S.M. Bernasconi), lukas.emmenegger@empa.ch (L. Emmenegger), msj@chem.ku.dk (M.S. Johnson), joachim.mohn@empa.ch (J. Mohn).

¹ These authors contributed equally to this work.

<https://doi.org/10.1016/j.aeaoa.2020.100094>

Received 5 August 2020; Received in revised form 25 September 2020; Accepted 27 September 2020

Available online 9 October 2020

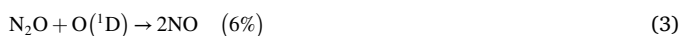
2590-1621/© 2020 The Authors.

Published by Elsevier Ltd.

This is an open access article under the CC BY-NC-ND license

(<http://creativecommons.org/licenses/by-nc-nd/4.0/>).

are shown in Eq. (1)–(3). Stratospheric photolysis in a narrow range of wavelengths (Eq. (1)) is by far the main removal path, constituting 90% of the total. The remaining 10% is removed by reaction with electronically excited oxygen atoms $O(^1D)$ (Eq. (2) and Eq. (3)), which are mainly produced in the atmosphere by photolysis of ozone (O_3) but also by photolysis of N_2O (Minschwaner et al., 1993).



The reaction of N_2O with $O(^1D)$ is the most important source of stratospheric NO_x gases which cause catalytic O_3 depletion.

The linear N_2O molecule (N–N–O) offers 12 different isotopocules, representing all possible combinations of naturally occurring isotopes of N and O (^{14}N , ^{15}N , ^{16}O , ^{17}O , ^{18}O). The abundances of individual isotopocules are often used to characterize sources and sinks of greenhouse gases (Peterson and Fry, 1987; Yu et al., 2020). To ease the isotopocule notation in this work, we make use of the HITRAN notation (Rothman et al., 2013), e.g. the shorthand 446 when referring to the $^{14}N^{14}N^{16}O$ isotopocule. The abundance of individual isotopocules is reported using the δ notation defined as

$$\delta^{xyz} = \frac{R_{\text{sample}}}{R_{\text{ref}}} - 1, \quad (4)$$

where the superscript xyz refers to one of the substituted isotopocules, and R is the ratio between the fraction of a substituted isotopocule to that of the most abundant species (446) for a sample and a reference (Toyoda and Yoshida, 1999). The $^{15}N/^{14}N$ ratios of Air- N_2 and $^{18}O/^{16}O$ and $^{17}O/^{16}O$ ratios of VSMOW are used as the reference scale. As the position of the two nitrogen atoms in the N_2O molecule is distinguishable, the ^{15}N site preference (SP) parameter is defined as (Toyoda et al., 2017)

$$SP = \delta^{456} - \delta^{546}. \quad (5)$$

“Clumped isotopes” is a collective term used for isotopocules containing more than one heavy isotope (Eiler, 2007). In this work, the three most abundant clumped isotopes in N_2O , isotopocules 458, 548, and 556, were studied. The isotopic quantities expressing deviation of their abundance from a stochastic (random) distribution, denoted as Δ^{458} , Δ^{548} , and Δ^{556} , are defined as (Kantnerová et al., 2020)

$$\Delta^{458} = \delta^{458} - \delta^{456} - \delta^{448}, \quad (6)$$

$$\Delta^{548} = \delta^{548} - \delta^{546} - \delta^{448}, \quad (7)$$

$$\Delta^{556} = \delta^{556} - \delta^{456} - \delta^{546}. \quad (8)$$

As with SP, the difference in the abundance of the clumped isotopomers 458 and 548 is defined as (Magyar et al., 2016)

$$SP^{18} = \delta^{458} - \delta^{548}. \quad (9)$$

A kinetic isotope effect describes a change in the rate of a chemical reaction for an isotopocule when its rate is larger or smaller due to isotopic substitution. Such an effect leads to the depletion or enrichment of the relative concentration of isotope or isotopocule in the sample as compared to the starting material. The kinetic isotope effect for an isotopocule xyz is commonly quantified via the fractionation constant ϵ_{xyz} or the fractionation factor α_{xyz} (Kaiser et al., 2003b), which are defined as

$$\alpha_{xyz} = \frac{k_{xyz}}{k_{446}} = 1 + \epsilon_{xyz}, \quad (10)$$

where k_{xyz} and k_{446} are reaction rate constants for one of the substituted

isotopocules and the most abundant species, respectively. Since the value of ϵ is small, it is usually reported in units of ‰.

The three-isotope exponent β is used to determine whether a process (e.g. photolysis) fractionates ^{17}O and ^{18}O in a mass-dependent way relative to ^{16}O (Kaiser et al., 2004). It is defined as

$$\beta = \frac{\ln(\epsilon_{447} + 1)}{\ln(\epsilon_{448} + 1)}, \quad (11)$$

where ϵ_{447} and ϵ_{448} are fractionation constants for isotopocules 447 and 448, respectively. A process is regarded to be anomalous in regard to O mass-dependent behavior if β is greater than 0.53 or lower than 0.50 (Schmidt et al., 2011).

The aim of this work is to determine isotopic fractionation of N_2O during photolysis by UV light. The absorption cross section of N_2O has its maximum around 180 nm (Selwyn et al., 1977). In the stratosphere, the spectrum of sunlight is highly structured in the range of N_2O absorption. There is a narrow UV window at roughly 205 nm, in between the absorption of O_3 and the Schumann-Runge band of molecular oxygen (O_2). Therefore, most N_2O is photolyzed on the low-energy shoulder of its absorption peak, in the spectral region 195–215 nm. Because of this alignment, a small shift in the position or intensity of the N_2O absorption, for example due to isotopic substitution, can have a large effect on the photolysis rate. Stratospheric processing leads to the enrichment of the heavier N_2O isotopocules in air returning from the stratosphere to the troposphere. This was first noted by Moore (1974) and confirmed later by Rahn and Wahlen (1997) and Kim and Craig (1993).

Experiments performed by Kaiser et al. (2003b) were used to study photolysis around the N_2O absorption maximum, at 185 nm, using a low-pressure Hg(Ar) light source. The fractionation constants were determined to be $(-18.6 \pm 0.5) \text{‰}$, $(3.7 \pm 0.2) \text{‰}$, and $(4.5 \pm 0.2) \text{‰}$ for 456, 546, and 448, respectively, while the fractionation constants increased to $(-95 \pm 7) \text{‰}$, $(-43 \pm 3) \text{‰}$, and $(-61 \pm 5) \text{‰}$ when photolysis was done with a Sb lamp and a bandpass filter around 220 nm. Other experimental studies of N_2O photolysis (Johnston et al., 1995; Rahn and Wahlen, 1997; Röckmann et al., 2000, 2001; Turatti et al., 2000; Umemoto, 1999; Zhang et al., 2000; Toyoda et al., 2018) are in qualitative agreement with the findings of Kaiser et al. (2003b). Von Hessberg et al. (2004) determined the temperature-dependent (233 K and 283 K) and wavelength-dependent (181–218 nm) cross section of 446, 546, 456, and 556. The data were used to construct fractionation constants with spectral resolution of 1 nm.

Yung and Miller (1997) introduced the theory that the absorption spectrum of an isotopically substituted species is that of the main component, shifted by the change in the vibrational zero-point energy (ZPE). Heavy isotope substitution shifts the absorption band to higher energy leading to reduced overlap with the stratospheric UV window. However, the ZPE-shift model underestimated isotopic fractionation compared to laboratory photolysis experiments by about a factor of two. Subsequent theoretical investigations by Johnson et al. (2001) and Schmidt et al. (2011) used quantum-mechanical wave packet propagation in connection with ground- and excited-state potential energy surfaces to study N_2O photolysis. The theoretical fractionation constants were in good agreement with values in the literature (Schmidt et al., 2011), and it was found that vibrational excitation in the bending mode is important for correct determination of the fractionation constants, especially at higher temperatures. Subsequent theoretical studies by Schmidt and Johnson (2015) extended and applied the method to determine fractionation constants for the multiply substituted species 556, 557, 458, 548, 457, and 547. Of these, experimental fractionation constants only exist for the 556 isotopocule (Kaiser et al., 2003a).

Recent development of improved laser spectroscopic (Kantnerová et al., 2019, 2020) and mass spectrometric techniques (Magyar et al., 2016) have enabled the first accurate measurements of low-abundance clumped N_2O isotopocules. These techniques are able to quantify the most abundant clumped isotopocules together with the singly

substituted and unsubstituted species in the same sample, even though their abundance spans a range of five orders of magnitude. They thus provide access to tracers that constrain the N₂O biogeochemical cycle. There is significant optimism that the additional information provided by these tracers will resolve critical gaps in our understanding of N₂O source mechanisms, source strengths, and atmospheric dynamics (Ostrom and Ostrom, 2017; Yu et al., 2020). In order to constrain the global N₂O budget, isotopic signatures and fractionation factors of the most important source and sink processes are required. It is therefore of paramount importance to determine the clumped isotope fractionation factors. This work presents experimentally determined fractionation constants for UV photolysis of the seven most abundant N₂O isotopocules (after 446), including, for the first time in one measurement setup, three clumped species, in the region of the stratospheric window.

2. Methodology

2.1. First principles calculation of photolytic fractionation

Isotopic fractionation constants at the temperature and wavelength of the experiments were derived from state-specific N₂O cross sections and the vibrational energies of the contributing vibrational states (ν_1 , ν_2 , ν_3) for the selected isotopocules as described in Schmidt et al. (2011). First, the total absorption cross section σ_{xyz} for an isotopocule xyz at photolysis wavelength λ and temperature T (20 °C) was calculated:

$$\sigma_{xyz}(\lambda, T) = \sum_i (w_i(T) \cdot \sigma_i(\lambda)), \quad (12)$$

where

$$w_i(T) = \frac{d_i}{Q(T)} \cdot e^{\frac{-E_i}{k_B T}} \quad (13)$$

is the Boltzmann weighting factor for each vibrational state i at temperature T , σ_i is the state-specific cross section for the isotopocule xyz at wavelength λ , d_i is the degeneracy of state i ($d = 1 + \nu_2$; ν_2 is the second vibrational quantum number associated with the N₂O bending mode), E_i is the vibrational energy of state i , k_B is Boltzmann's constant, and Q is the partition function:

$$Q(T) = \sum_i \left(d_i \cdot e^{\frac{-E_i}{k_B T}} \right). \quad (14)$$

The expected fractionation constant ϵ_{xyz} for an isotopocule xyz was calculated following Eq. (15):

$$\epsilon_{xyz}(\lambda, T) = \frac{\sigma_{xyz}(\lambda, T)}{\sigma_{446}(\lambda, T)} - 1. \quad (15)$$

The input data for the calculation were acquired from supplementary material related to work by Schmidt et al. (2011) for all species except 458 and 548, for which the data were obtained following personal communication with J. A. Schmidt.

2.2. UV photolysis

The photolysis experiments were performed in a custom-made cylindrical stainless-steel reactor with inner diameter of 5.7 cm, base length of 44 cm, and volume of 1.1 L. Both ends of the photoreactor were equipped with uncoated fused-silica windows (Thorlabs, USA) with high transmission in the region 185–2100 nm. The photoreactor was equipped with a pressure gauge (LEO3, 0–1 MPa, Keller AG, Switzerland) to monitor the gas pressure during the experiment. It was filled with a N₂O gas mixture (high purity N₂O – 99.999%, PanGas, The Linde Group, Switzerland – diluted with 99.9999% N₂ to 1.70% N₂O by NPL, Teddington, UK) to a pressure of 300 kPa. The pressure in the photolysis cell decreased gradually during the experiment as samples of the gas were

extracted for analysis, and also due to a minor leak to the ambient air. The pressure in the photoreactor was not allowed to drop below 140 kPa to ensure stable sampling conditions.

Photolysis was driven by a broadband laser-driven Xe-plasma light source (LDLS EQ-99, Energetiq, USA) that produces a stable output in the range of 170–2100 nm. Stratospheric behavior was simulated by illuminating the cell in two regions selected with dielectric bandpass filters (Edmund Optics, USA) placed between the light source and the photoreactor: the bandpass filters were centered at 200 nm and 214 nm with a full width at half maximum (FWHM) of 10 nm and a peak transmission of 18–20%. The light source output was collimated before hitting the bandpass filter. The photolysis experiments were run for around 9 days using the filter at 200 nm and 28 days using the filter at 214 nm (photolysis yields are specified in the Results and Discussion). The experiment with the bandpass filter at 200 nm was duplicated. The progress of the photolysis was traced by measuring concentration of residual N₂O in the photoreactor by QCLAS.

The relative stability of the light source was confirmed to be better than 5% over the full emission spectrum by regular analysis of the light exiting the photoreactor with a UV/NIR spectrometer (Flame-S-XR1-ES, Ocean Optics, USA). Relative spectral photolysis rates shown in Fig. 1b were calculated by combining transmittance curves of the bandpass filters with the cross section of 446 calculated by Schmidt et al. (2011), which are shown in Fig. 1a. The maximum of the relative photolysis rate spectrum is shifted by 1–2 nm relative to the transmittance curves of the corresponding bandpass filters due to the slope of the absorption cross section. Therefore, the theoretical fractionation constants in Table 1 and Table 2 were calculated at the wavelength of the maximum photolysis rate – 198 nm and 213 nm – and not the center of the filter passband. Including the entire band in the calculation of the theoretical fractionation constants changed the results by less than 1 ‰. Therefore, the fractionation constants calculated at the single wavelength of the maximum photolysis rate were directly compared to the fractionation constants obtained using the bandpass filters that transmit a given wavelength region.

2.2.1. Secondary effects

Kaiser et al. (2002b) observed that the apparent fractionation constants decreased in experiments when the degree of photolysis was high. This was explained by the build-up of photolysis products, e.g. NO₂ and O₃, which led to a secondary source of O(¹D) in the experiment. Following Kaiser et al. (2002b), a box model was created for this study to estimate the effect of secondary chemistry in the photolysis experiment. According to the model, approximately 6–9% of N₂O is removed by O(¹D). Most of this loss is due to O(¹D) produced directly in N₂O photolysis.

A blank experiment (without photolysis) was performed for 14 days with sampling every 24 h to test the stability of the instrument and potential secondary effects (e.g. leakage) in the photoreactor over extended periods. We found a subtle decrease of N₂O concentration during the course of the blank experiment, but no change in the N₂O isotopic composition, and attributed the N₂O loss to a possible catalytic decomposition or minor leakage during sampling. This loss was corrected in all experiments, although it was minor. Based on the box model, the rate of this secondary N₂O loss was determined to be one order of magnitude lower than the photolysis rate at 214 nm and two orders of magnitude lower than the photolysis rate at 200 nm.

The box model was also used to estimate the ratio of N₂O removed by photolysis itself as shown in Appendix, Fig. A1: 92% and 78% is removed by photolysis in the 200 nm and 214 nm experiments, respectively, and the rest is removed by secondary chemistry. The fractionation constants for the N₂O + O(¹D) reaction were determined by Kaiser et al. (2002a) to be (– 2.21 ± 0.12) ‰, (– 8.79 ± 0.14) ‰, and (– 12.23 ± 0.14) ‰ for the isotopocules 456, 546, and 448, respectively. Secondary loss in the 200 nm experiment is < 8% (2% caused by loss

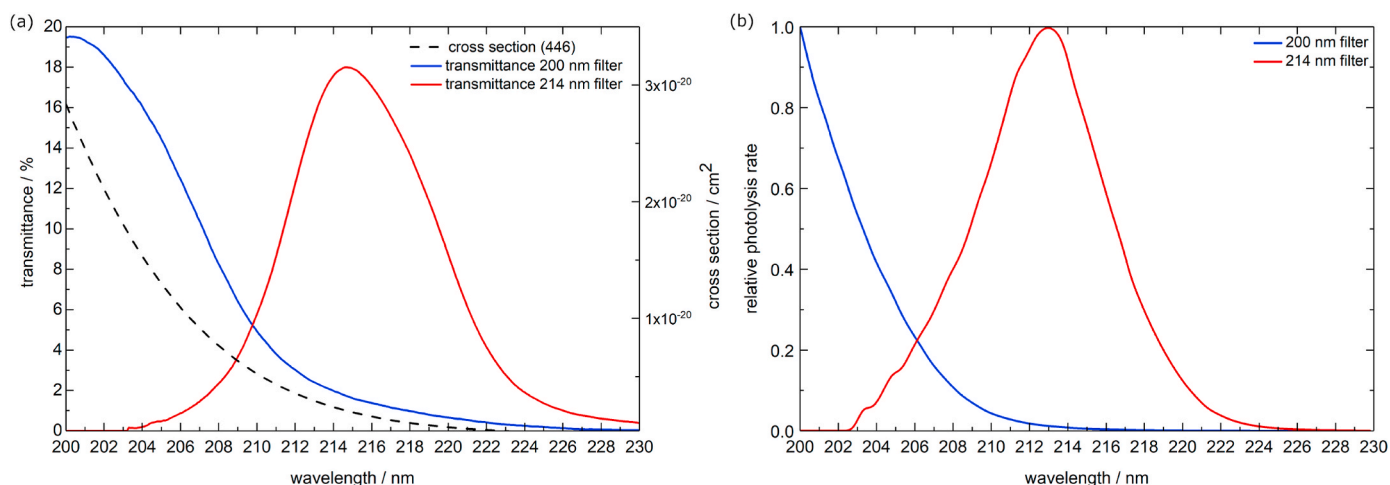


Fig. 1. (a) Transmittance of the bandpass filters and 446 absorption cross section from Schmidt et al. (2011). (b) Relative photolysis rates for the bandpass filters. The relative photolysis rate is calculated by multiplying the transmission with the absorption cross section and dividing all values by the value at peak maximum.

Table 1

Fractionation constants ϵ for photolysis of N_2O with the 200 nm bandpass filter at 20 °C calculated by two different methods (described in the main text) – “mean direct” and “Rayleigh plot”; fractionation constants ϵ derived from theoretical absorption cross sections at 20 °C based on Schmidt et al. (2011) (theory); and experimental values of Kaiser et al. (2003b) at room temperature (experiment). The uncertainty is expressed at the 95% confidence interval based on uncertainties of the duplicate experiments. All values are given in ‰.

	“mean direct”	“Rayleigh plot”	theory	experiment
	ϵ	ϵ	intercept	ϵ
ϵ_{456}	-51.6 ± 4.8	-48.9 ± 7.4	0.3 ± 0.4	-45.6
ϵ_{546}	-25.2 ± 3.8	-22.8 ± 5.3	0.2 ± 0.3	-21.0
$\epsilon_{15\text{bulk}}$	-38.4 ± 3.0	-35.5 ± 4.7	0.3 ± 0.2	-33.3
ϵ_{447}	-11.7 ± 3.1	-12.7 ± 4.5	-0.1 ± 0.2	-15.5
ϵ_{448}	-31.1 ± 8.5	-33.5 ± 12.0	0.1 ± 0.6	-29.3
ϵ_{458}	-78.8 ± 4.5	-80.9 ± 6.5	-0.1 ± 0.3	-61.2
ϵ_{548}	-51.3 ± 7.3	-52.7 ± 10.8	0.1 ± 0.5	-39.5
ϵ_{556}	-68.7 ± 7.6	-66.9 ± 9.8	0.4 ± 0.4	-66.7

Table 2

Fractionation constants ϵ for photolysis of N_2O with the 214 nm bandpass filter at 20 °C calculated by two different methods (described in the main text) – “mean direct” and “Rayleigh plot”; fractionation constants ϵ derived from theoretical absorption cross sections at 20 °C based on Schmidt et al. (2011) (theory); and experimental values of Kaiser et al. (2003b) at room temperature (experiment). The uncertainty is expressed at the 95% confidence interval. All values are given in ‰.

	“mean direct”	“Rayleigh plot”	theory	experiment
	ϵ	ϵ	intercept	ϵ
ϵ_{456}	-88 ± 1.7	-82.4 ± 22.3	0.2 ± 0.5	-83.5
ϵ_{546}	-42.1 ± 18.7	-36.1 ± 19.6	0.3 ± 0.4	-45.2
$\epsilon_{15\text{bulk}}$	-65.1 ± 12.9	-59.0 ± 15.0	0.3 ± 0.3	-64.4
ϵ_{447}	-29.8 ± 14.9	-21.9 ± 15.7	0.4 ± 0.3	-37.6
ϵ_{448}	-48.9 ± 25.4	-44.1 ± 29.8	0.2 ± 0.6	-70.3
ϵ_{458}	-130.4 ± 20.3	-120.9 ± 23.7	0.0 ± 0.5	-92.4
ϵ_{548}	-81.6 ± 22.6	-79.1 ± 28.5	0.2 ± 0.6	-59.7
ϵ_{556}	-112.9 ± 23.5	-110.9 ± 27.5	0.1 ± 0.6	-124.3

determined from the blank experiment, 6% caused by the $\text{N}_2\text{O} + \text{O}(^1\text{D})$ reaction), whereas for the 214 nm experiment it is < 22% (13% caused by loss determined from the blank experiment, 9% caused by the $\text{N}_2\text{O} +$

$\text{O}(^1\text{D})$ reaction; these fractions were determined from the box model). Therefore, the effect of the $\text{N}_2\text{O} + \text{O}(^1\text{D})$ reaction on the fractionation constant of N_2O photolysis is small (max. 0.2 ‰ for 456, 0.8 ‰ for 546, 1.1 ‰ for 448). Moreover, information regarding the fractionation of the other studied isotopocules for this reaction is not available. Consequently, in this work we assume that the $\text{O}(^1\text{D})$ loss process and the N_2O loss observed during the blank experiment do not fractionate isotopes (similarly to Kaiser et al., 2003a) and photolysis of N_2O is the only process responsible for the observed isotopic fractionation.

2.3. QCLAS analysis

The analytical setup includes a quantum cascade laser absorption spectrometer (QCLAS, Aerodyne Research, Inc., USA; Kantnerová et al., 2020) and a customized automated inlet system (Aerodyne Research, Inc., USA). The QCLAS instrument is equipped with an astigmatic Herriott multi-pass absorption cell (volume 2.5 L, optical path length 204 m). Samples are measured at a pressure of 400 Pa. The inlet system consists of a 16-port VICI rotary valve (VICI Valco Instruments, USA), 10 pneumatically operated bellows valves (BK series, Swagelok, USA), a high-conductance pneumatic valve (Swagelok, USA), a pressure sensor (0–130 kPa Baratron, MKS Instruments, USA), and a turbo-molecular pump station (HiCube 80 Eco, Pfeiffer Vacuum (Schweiz) AG, Switzerland). It is operated by command-based scripts in the TDLWintel software that controls the QCLAS instrument.

The inlet system introduces calibration or sample gas (approx. 10 mL at standard temperature and pressure) into the optical cell of the QCLAS instrument. Pressure in the optical cell is controlled by subsampling of the analyzed gas into an intermediate volume of 50 mL (± 20 mL). Prior to filling, the VICI valve and the tubing are purged with the analyzed gas to the pump station. Then, the gas is expanded into the optical cell, the cell is closed, and an absorption spectrum is measured. A measurement cycle consists of analysis of a sample bracketed by analyses of three calibration gases and requires around 40 min. Between the individual measurements, the optical cell and the inlet system are evacuated for 90 s, flushed with nitrogen, and evacuated for another 90 s.

The sampling scheme was adapted to the strongly different photolysis rate at 200 nm and 214 nm. When using the 200 nm bandpass filter, the gas was sampled every 12 h for the full duration of the experiment. For the experiment at 214 nm, sampling took place every 12 h for the first 4 days, then once per week (triplicates) until day 28, when the sample gas analysis was run four times.

Three calibration gases span the concentration range of 1.50–1.85% N_2O in N_2 (Kantnerová et al., 2020). They share the same isotopic composition: $\delta^{456} = (-0.11 \pm 0.20) \text{ ‰}$, $\delta^{546} = (0.95 \pm 0.21) \text{ ‰}$,

$\delta^{448} = (38 \pm 0.25) \text{ ‰}$, $\Delta^{458} = (-0.06 \pm 0.80) \text{ ‰}$, $\Delta^{548} = (0.49 \pm 0.46) \text{ ‰}$, $\Delta^{556} = (-0.88 \pm 1.76) \text{ ‰}$. The uncertainties are given at the 95% confidence interval.

2.4. Data analysis

The δ^{xyz} (Eq. (4)) and Δ^{xyz} (Eq. (6)–(8)) values for an isotopocule xyz were calculated using a mole fraction-calibration scheme described in Kantnerová et al. (2020). The full definitions for the isotopic values can be found therein. The isotopic composition of the calibration gases reported in section 2.3 is used for the calculations.

The time evolution of the δ values during photolysis was described by the Rayleigh distillation model following Schmidt et al. (2011) (Eq. (16)) in its linearized form (Eq. (17)):

$$\delta^{xyz} = \left(\frac{R_0^{xyz}}{R_{ref}^{xyz}} \right) \cdot f^{\epsilon_{xyz}} - 1, \quad (16)$$

$$\ln \left(\frac{\delta^{xyz} + 1}{\delta_0^{xyz} + 1} \right) = \epsilon_{xyz} \cdot \ln(f), \quad (17)$$

where R_0^{xyz} is the initial ratio of the isotopocule xyz and 446 in the photolyzed gas (represented by δ_0^{xyz} in Eq. (17)), R_{ref}^{xyz} is the ratio of the reference (VSMOW for $^{17}\text{O}/^{16}\text{O}$ and $^{18}\text{O}/^{16}\text{O}$ and Air-N₂ for $^{15}\text{N}/^{14}\text{N}$), f is the remaining fraction of unphotolyzed isotopocule 446, and ϵ_{xyz} is the fractionation constant.

The fractionation constants ϵ were calculated by two different strategies, following Kaiser et al. (2003b): 1) “Rayleigh plot” – weighted least-squares regression using Eq. (17) in the form $y = a \cdot x + b$ assuming an error in both variables (derived from the experimental precision; York et al., 2004); 2) “mean direct” method – only the five last measurements were considered ($f < 0.093$) and the intercept (b) was set to zero. The slope a and the intercept b of the regression fit were calculated with 95% confidence intervals.

3. Results and Discussion

Using the bandpass filter at 200 nm, 8.8% of the initial N₂O amount was photolyzed during the two 9-day experiments. For the bandpass filter at 214 nm, 4.6% of the initial N₂O amount was photolyzed in 28 days. Fig. 2 shows an example of the Rayleigh fractionation plots for δ^{458} and $\delta^{15}\text{N}^{\text{bulk}}$ in panel (a), and δ^{556} and δ^{447} in panel (b). Clearly, the doubly substituted isotopocules undergo stronger photolytic fractionation than the singly substituted isotopocules (Fig. 2). Observed smaller

photolysis rates for the heavier isotopocules in comparison with the lighter isotopocules indicate a so-called normal isotope effect.

The fractionation constants determined by the UV photolysis experiments with the 200 nm and 214 nm bandpass filters are shown in Tables 1 and 2, respectively. ϵ values for both calculation strategies are in agreement within their uncertainty, which is generally smaller for the “mean direct” approach. The uncertainty for the photolysis experiment at 214 nm is larger than at 200 nm because of the about twofold lower photolysis rate.

Furthermore, Table 1 and Table 2 compare the fractionation constants from our study with those from Kaiser et al. (2003b), both at room temperature, and values calculated using absorption cross sections at 20 °C. Our results agree with the theoretical values for most isotopocules, and for all isotopocules with the values from Kaiser et al. (2003b) within the experimental uncertainty. The fractionation constants of the isotopocule 448 at 214 nm are somewhat smaller than the theoretical values but they agree well with the value by Kaiser et al. (2003b). However, our experimental values for the clumped isotopomers 458 and 548 are consistently larger than the theoretical values, meaning that photolysis of these species is slower than is predicted by the aforementioned theory.

According to Kaiser et al. (2003a), the fractionation constant ϵ_{556} must be equal to the sum of the fractionation constants at the central and terminal N positions (ϵ_{456} and ϵ_{546} , respectively) in order to maintain a statistical isotope distribution. Based on the available experimental evidence, those authors noted that this “additivity rule” seemed to be valid, although the value of ϵ_{556} predicted from the sum of ϵ_{456} and ϵ_{546} obtained experimentally in their work deviated significantly from the observed ϵ_{556} at two of the seven data points, by 20–30 %. The remaining five data points were in agreement to within the error of the measurement. In addition, theoretical predictions using the ZPE models (Yung and Miller, 1997) seemed to confirm the additivity rule. However, later theoretical predictions employing more complete models do not obey this rule (Johnson et al., 2001; Schmidt et al., 2011; Schmidt and Johnson, 2015). There is no strong theoretical argument for the additivity rule because many of the underlying processes are nonlinear, including the shift in ZPE with isotopic substitution, and the amplitude of the bending motion, which affects the transition amplitude as the transition dipole changes strongly with the bending angle. Moreover, isotopic substitution influences both the amplitude and the energy of the transition, in addition to changing the populations of the vibrational states, most importantly the bending state (Nanbu and Johnson, 2004).

For completeness, we applied the additive rule to the new species explored in this paper because, as stated in Kaiser et al. (2003a), the additivity rule observed for 556 should apply also to other doubly

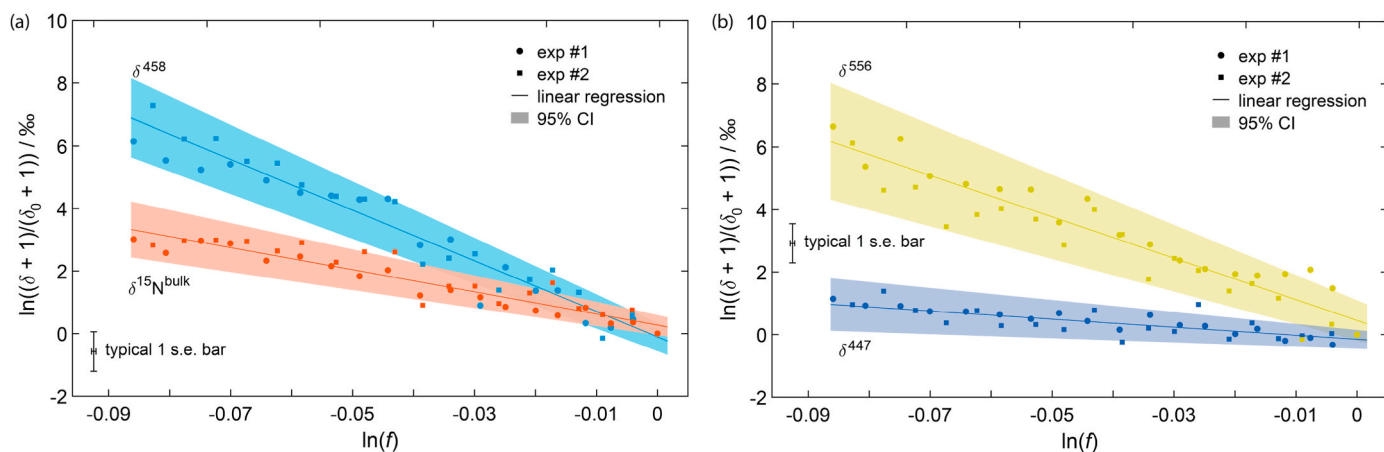


Fig. 2. Rayleigh fractionation plots of $\ln((\delta + 1)/(\delta_0 + 1))$ vs. $\ln(f)$ for photolysis with the 200 nm bandpass filter. (a) δ^{458} and $\delta^{15}\text{N}^{\text{bulk}}$, (b) δ^{556} and δ^{447} . The experimental data were fitted by using a linear regression function $y = a \cdot x + b$, assuming an error in both variables (typical 1 standard error (s.e.) bar depicted). Shaded areas show the 95% confidence intervals.

substituted isotopocules. Based on the values shown in Tables 1 and 2, the additivity rule is, within the experimental uncertainty, consistent for the experimental results for all three clumped isotopocules and for the theoretical value of ϵ_{556} , but not for those of ϵ_{458} and ϵ_{548} . More work needs to be performed in order to resolve the discrepancy between the experimental and theoretical results for the species 458 and 548. Experimental determination of the absorption cross section of the two species can provide an alternative approach to access the fractionation constant and may likely resolve the discrepancy. The observed discrepancy may be linked to secondary reactions occurring along the photolysis, or possibly the theoretical potential energy surfaces used in Schmidt et al. (2011) could be improved by a higher level of theory and a tighter computational grid.

Experimental values of the three-isotope exponent β_{exp} were calculated based on Eq. (11) using the “Rayleigh plot”-derived values of ϵ in Tables 1 and 2, and compared with theoretical values of β_{theory} , which are based on the expected values of ϵ . The values of β_{exp} are within their uncertainty intervals (1 σ) in agreement with β_{theory} : $\beta_{\text{exp}}(200 \text{ nm}) = 0.46 \pm 0.16$, $\beta_{\text{theory}}(200 \text{ nm}) = 0.52$, $\beta_{\text{exp}}(214 \text{ nm}) = 0.49 \pm 0.25$, $\beta_{\text{theory}}(214 \text{ nm}) = 0.53$. The obtained larger uncertainty of β_{exp} prevents stating with confidence that the photolytic fractionation was mass-dependent for ^{17}O and ^{18}O relative to ^{16}O .

During photolysis at both wavelengths, SP and SP¹⁸ show small temporal trends – approx. 2 ‰ for SP and 4 ‰ for SP¹⁸. This corresponds to larger values of the fractionation constant ϵ for the isotopocules 546 and 548 in comparison to 456 and 458, respectively. In other words, the isotopocules 546 and 548 are photolyzed faster than their corresponding isotopomer, causing the gradual change in SP and SP¹⁸.

The Δ values of the clumped isotopocules do not show any significant change in the course of photolysis. Δ^{458} is slightly enriched compared to the stochastic distribution, with values up to 4 ‰. On the contrary, Δ^{548} has slightly negative values, down to – 4 ‰, similarly to Δ^{556} , which is between – 2 and – 1 ‰. The standard uncertainty of the Δ values is approx. 1 ‰.

4. Conclusion

The experiments simulated the major sink of N₂O in the stratosphere, where N₂O is removed by UV light in the transmission window (195–215 nm). The photolysis experiments with the 200 nm and 214 nm bandpass filters allow the determination of fractionation constants of both singly and doubly substituted isotopocules of N₂O. The photolysis rate at 200 nm is larger than at 214 nm. The fractionation constants,

based on laser spectroscopic measurements of residual N₂O, indicate slower photolysis progress for the isotopically substituted species in comparison with the lighter species 446, or a so-called normal isotope effect.

Most of the fractionation constants obtained in this study (for isotopocules 456, 546, 447, 448, and 556) show good agreement for both photolysis wavelengths with values calculated from theoretical absorption cross sections by Schmidt et al. (2011) and experimental values for the singly substituted species determined by Kaiser et al. (2003b). Fractionation constants obtained for the clumped isotopomers 458 and 548 show a discrepancy with respect to the theoretical values. This may lead to a refinement of possible secondary chemistry or of theoretical predictions for the clumped isotopes in N₂O, and ultimately improve the quantification of the importance of UV photolysis in the stratospheric N₂O budget. Finally, our experiments show that the effect of stratospheric photolysis on the clumped isotope Δ values of tropospheric N₂O is modest, and therefore any variation that is seen will be strongly characteristic of the source and not of atmospheric processes.

CRediT authorship contribution statement

Kristýna Kantnerová: Data curation, Formal analysis, Investigation, Methodology, Writing - original draft. **Malte F. Jespersen:** Data curation, Formal analysis, Investigation, Methodology, Writing - original draft. **Stefano M. Bernasconi:** Supervision, Writing - review & editing. **Lukas Emmenegger:** Supervision, Writing - review & editing. **Matthew S. Johnson:** Methodology, Supervision, Writing - review & editing. **Joachim Mohn:** Methodology, Supervision, Writing - review & editing.

Declaration of competing interest

The authors declare that they have no known competing financial interests or personal relationships that could have appeared to influence the work reported in this paper.

Acknowledgement

This work was supported by the Swiss National Science Foundation (Grant 200021_166255). We would like to thank J. A. Schmidt for providing us with data of state-specific cross sections and vibrational energies for isotopocules 458 and 548. We would like to thank I. Prokhorov for helping with the setup of the photolysis experiment.

Appendix

A. Box model

A box model was created to estimate the effect of secondary chemistry in the photolysis experiment. The starting conditions of the box model are shown in Table A1. The bi- and termolecular reactions included in the model are listed in Table A2. The photolysis rate of N₂O is estimated by fitting the time evolution of N₂O to the experimental data as shown in Fig. A2. All other photolysis rates are estimated using the ratio between the absorption cross section of the species and that of N₂O. The absorption cross sections are shown in Tables A3 and A4, and the photolysis rates in Tables A5 and A6. Radical wall loss is calculated from a 2D-diffusion model, where the diffusion length D_l of the considered radical species is calculated from Eq. (A1):

$$D_l = \sqrt{4D_x t}, \quad (\text{A1})$$

where D_x is the diffusion constant and t is the time. The gas mixture is assumed to be a binary gas mixture with N₂ as the only bath gas. The diffusion constant D_x is calculated as:

$$D_x = \frac{3}{8p\sigma_x^2} \sqrt{\frac{k_B^3 T^3}{2\pi} \left(\frac{1}{m_x} + \frac{1}{m_{\text{N}_2}} \right)}, \quad (\text{A2})$$

where p is the pressure, σ_x is the average cross section of the two components, and m_x and m_{N_2} are the molecular masses of the radical and molecular

nitrogen, respectively. The average cross sections are calculated from crude estimates of van der Waals radii obtained by molecular mechanic optimization in the GaussView software. The values of the van der Waals radii are shown in Table A7. The N₂O removal observed in the blank experiment is included as wall loss in the box model. Experimental and modeled N₂O loss in the blank experiment are shown in Fig. A3. Loss due to sampling is calculated from an exponential fit to the starting and end pressure and is shown in Tables A8 and A9.

A sensitivity analysis was performed on the box model. Four critical parameters – pressure, photolysis rate, water concentration, and radical wall loss – were selected to test the performance of the box model. The starting pressure and the photolysis rates were varied by $\pm 10\%$. The initial water concentrations of 0, 1, 10 and 100 $\mu\text{mol mol}^{-1}$ were tested. The radical wall loss was increased by a factor of 10 and excluded entirely from the model. The results of this analysis are shown in Table A10 and indicate that the uncertainties in the 214 nm experiment are higher than in the 200 nm experiment. In addition, the uncertainty for the determined fraction of N₂O that reacts by photolysis is lower than $\pm 1.5\%$, showing that two major contributions to the secondary chemistry are O(¹D) directly formed by N₂O photolysis and the N₂O loss observed in the blank experiment. The results indicate that secondary chemistry has only a minor effect on the results under the small extent of photolysis obtained in this work, but may become important when higher extents of photolysis are reached. The build-up of photolysis products during the photolysis experiments are shown in Fig. A4 and Fig. A5. The build-up of O₃ and O₂ especially is a potential source of O(¹D), thereby leading to an increased removal of N₂O in the experiment.

Table A1

Initial concentration of species included in the box model, species not listed in the table have initial concentration of 0 molecules/cm³

200 nm	molecules/cm ³
N ₂	$7.37 \cdot 10^{19}$
N ₂ O	$1.26 \cdot 10^{18}$
H ₂ O	$7.5 \cdot 10^{14}$
214 nm	molecules/cm ³
N ₂	$7.50 \cdot 10^{19}$
N ₂ O	$1.28 \cdot 10^{18}$
H ₂ O	$7.6 \cdot 10^{14}$

Table A2

Secondary bi- and termolecular reactions included in the box model

termolecular/(cm ⁶ s ⁻¹)	E _a /(kJ mol ⁻¹)	reaction	reference
$9.98 \cdot 10^{-32}$	0.00	OH + NO ₂ + M → HNO ₃ + M	Sander et al. (2011)
$2.61 \cdot 10^{-31}$	0.00	O(³ P) + NO ₂ + M → NO ₃ + M	Sander et al. (2011)
$2.86 \cdot 10^{-36}$	0.00	O(¹ D) + N ₂ + M → N ₂ O + M	Sander et al. (2011)
$9.32 \cdot 10^{-32}$	0.00	O(³ P) + NO + M → NO ₂ + M	Sander et al. (2011)
$4.27 \cdot 10^{-36}$	0.00	H + O ₂ + M → HO ₂ + M	Sander et al. (2011)
$5.20 \cdot 10^{-35}$	- 7.48	O(³ P) + O(³ P) + M → O ₂ + M	Tsang and Hampson (1986)
$6.35 \cdot 10^{-34}$	0.00	O ₂ + O(³ P) + M → O ₃ + M	Sander et al. (2011)
bimolecular/(cm ³ s ⁻¹)	E _a /(kJ mol ⁻¹)	reaction	reference
$3.12 \cdot 10^{-11}$	- 0.46	O ₂ + O(¹ D) → O ₂ + O(³ P)	Sander et al. (2011)
$8.00 \cdot 10^{-12}$	17.13	O ₃ + O(³ P) → 2O ₂	Sander et al. (2011)
$1.20 \cdot 10^{-10}$	0.00	O ₃ + O(¹ D) → 2O ₂	Sander et al. (2011)
$1.20 \cdot 10^{-10}$	0.00	O ₃ + O(¹ D) → O ₂ + 2O(³ P)	Sander et al. (2011)
$2.15 \cdot 10^{-11}$	- 0.91	O(¹ D) + N ₂ → N ₂ + O(³ P)	Sander et al. (2011)
$4.63 \cdot 10^{-11}$	- 0.17	N ₂ O + O(¹ D) → N ₂ + O ₂	Sander et al. (2011)
$7.25 \cdot 10^{-11}$	- 0.17	N ₂ O + O(¹ D) → 2 NO	Sander et al. (2011)
$5.10 \cdot 10^{-12}$	- 1.75	NO ₂ + O(³ P) → NO + O ₂	Sander et al. (2011)
$1.00 \cdot 10^{-11}$	0.00	O(³ P) + NO ₃ → O ₂ + NO ₂	Sander et al. (2011)
$3.00 \cdot 10^{-12}$	12.47	NO + O ₃ → NO ₂ + O ₂	Sander et al. (2011)
$1.50 \cdot 10^{-11}$	- 1.41	NO + NO ₃ → 2 NO ₂	Sander et al. (2011)
$1.20 \cdot 10^{-13}$	20.37	NO ₂ + O ₃ → NO ₃ + O ₂	Sander et al. (2011)
$8.50 \cdot 10^{-13}$	20.37	NO ₃ + NO ₃ → 2NO ₂ + O ₂	Sander et al. (2011)
$1.44 \cdot 10^{-12}$	0.00	NO ₂ + NO ₃ → N ₂ O ₅	Sander et al. (2011)
$2.00 \cdot 10^{-21}$	0.00	N ₂ O ₅ + H ₂ O → 2HNO ₃	Sander et al. (2011)
$1.63 \cdot 10^{-10}$	- 0.49	O(¹ D) + H ₂ O → 2OH	Sander et al. (2011)
$1.80 \cdot 10^{-11}$	- 1.50	O(³ P) + OH → O ₂ + H	Sander et al. (2011)
$3.00 \cdot 10^{-11}$	- 1.66	O(³ P) + HO ₂ → OH + O ₂	Sander et al. (2011)
$1.40 \cdot 10^{-10}$	3.91	H + O ₃ → OH + O ₂	Sander et al. (2011)
$7.20 \cdot 10^{-11}$	0.00	H + HO ₂ → 2OH	Sander et al. (2011)
$1.60 \cdot 10^{-12}$	0.00	H + HO ₂ → O(³ P) + H ₂ O	Sander et al. (2011)
$6.90 \cdot 10^{-12}$	0.00	H + HO ₂ → H ₂ + O ₂	Sander et al. (2011)
$1.70 \cdot 10^{-12}$	7.82	OH + O ₃ → HO ₂ + O ₂	Sander et al. (2011)
$2.80 \cdot 10^{-12}$	14.97	OH + H ₂ → H ₂ O + H	Sander et al. (2011)
$1.80 \cdot 10^{-12}$	0.00	OH + OH → H ₂ O + O(³ P)	Sander et al. (2011)
$2.60 \cdot 10^{-11}$	0.00	OH + OH → H ₂ O ₂	Sander et al. (2011)
$4.80 \cdot 10^{-11}$	- 2.08	OH + HO ₂ → H ₂ O + O ₂	Sander et al. (2011)
$1.80 \cdot 10^{-12}$	0.00	OH + H ₂ O ₂ → H ₂ O + HO ₂	Sander et al. (2011)
$1.00 \cdot 10^{-14}$	4.07	HO ₂ + O ₃ → OH + 2O ₂	Sander et al. (2011)

(continued on next page)

Table A2 (continued)

termolecular/(cm ⁶ s ⁻¹)	E _a /(kJ mol ⁻¹)	reaction	reference
3.00 · 10 ⁻¹³	– 3.82	HO ₂ + HO ₂ → H ₂ O ₂ + O ₂	Sander et al. (2011)
1.40 · 10 ⁻¹²	16.63	O(³ P) + H ₂ O ₂ → OH + HO ₂	Sander et al. (2011)
3.60 · 10 ⁻¹¹	0.00	OH + NO → HONO	Sander et al. (2011)
1.80 · 10 ⁻¹¹	3.24	OH + HONO → H ₂ O + NO ₂	Sander et al. (2011)
1.64 · 10 ⁻¹³	0.00	OH + HNO ₃ → H ₂ O + NO ₃	Sander et al. (2011)
2.90 · 10 ⁻¹²	0.00	HO ₂ + NO ₂ → HO ₂ NO ₂	Sander et al. (2011)
5.00 · 10 ⁻¹⁶	0.00	HO ₂ + NO ₂ → HONO + O ₂	Sander et al. (2011)
3.50 · 10 ⁻¹²	0.00	HO + NO ₃ → OH + NO ₂ + O ₂	Sander et al. (2011)
4.00 · 10 ⁻¹⁰	2.83	H + NO ₂ → OH + NO	Sander et al. (2011)
2.20 · 10 ⁻¹¹	0.00	OH + NO ₃ → NO ₂ + HO ₂	Sander et al. (2011)

Table A3

Absorption cross sections used in the model for the 200 nm experiment

species	wavelength/nm	cross section/cm ²	quantum yield	reference
O ₃ → O ₂ + O(¹ D)	198–202	3.20 · 10 ⁻¹⁹	1	Sander et al. (2011)
N ₂ O → N ₂ + O(¹ D)	200–202	3.84 · 10 ⁻²⁰	1	Sander et al. (2011)
O ₂ → 2O(³ P)	205	7.25 · 10 ⁻²⁴	1	Sander et al. (2011)
N ₂ O ₅ → NO ₃ + NO + O(³ P)	200	9.10 · 10 ⁻¹⁸	1	Sander et al. (2011)
NO ₃ → NO ₂ + O(¹ D)	220	3.4 · 10 ⁻¹⁹	1	Sander (1986)
HO ₂ → OH + O(¹ D)	200	3.68 · 10 ⁻¹⁸	1	Sander et al. (2011)
H ₂ O → OH + H	198	9.00 · 10 ⁻²²	1	Sander et al. (2011)
H ₂ O ₂ → 2OH	200	4.75 · 10 ⁻¹⁹	1	Sander et al. (2011)
HONO → H + NO ₂	200	2.10 · 10 ⁻¹⁸	1	Sander et al. (2011)
HNO ₃ → OH + NO ₂	200	5.88 · 10 ⁻¹⁸	0.33	Sander et al. (2011)
HNO ₃ → HONO + O(¹ D)	200	5.88 · 10 ⁻¹⁸	0.67	Sander et al. (2011)
HO ₂ NO ₂ → OH + NO ₃	200	5.63 · 10 ⁻¹⁸	0.25	Sander et al. (2011)
HO ₂ NO ₂ → HO ₂ + NO ₂	200	5.63 · 10 ⁻¹⁸	0.75	Sander et al. (2011)

Table A4

Absorption cross sections used in the model for the 214 nm experiment

species	wavelength/nm	cross section/cm ²	quantum yield	reference
O ₃ → O ₂ + O(¹ D)	212.77–215.05	9.03 · 10 ⁻¹⁹	1	Sander et al. (2011)
N ₂ O → N ₂ + O(¹ D)	214	3.42 · 10 ⁻²¹	1	Sander et al. (2011)
O ₂ → 2O(³ P)	214	5.72 · 10 ⁻²⁴	1	Sander et al. (2011)
N ₂ O ₅ → NO ₃ + NO + O(³ P)	214	3.22 · 10 ⁻¹⁸	1	Sander et al. (2011)
NO ₂ → NO + O(¹ D)	214	4.64 · 10 ⁻¹⁹	1	Bass et al. (1976)
NO ₃ → NO ₂ + O(¹ D)	220	3.4 · 10 ⁻¹⁹	1	Sander (1986)
HO ₂ → O(¹ D) + OH	215	3.85 · 10 ⁻¹⁸	1	Sander et al. (2011)
H ₂ O ₂ → 2 OH	215	3.07 · 10 ⁻¹⁹	1	Sander et al. (2011)
N ₂ O ₅ → NO ₃ + NO + O(³ P)	214	3.22 · 10 ⁻¹⁸	1	Sander et al. (2011)
HONO → H + NO ₂	214	1.93 · 10 ⁻¹⁸	1	Sander et al. (2011)
HNO ₃ → OH + NO ₂	214	4.39 · 10 ⁻¹⁹	0.33	Sander et al. (2011)
HNO ₃ → HONO + O(¹ D)	214	4.39 · 10 ⁻¹⁹	0.67	Sander et al. (2011)
HO ₂ NO ₂ → OH + NO ₃	215	1.61 · 10 ⁻¹⁸	0.25	Sander et al. (2011)
HO ₂ NO ₂ → HO ₂ + NO ₂	215	1.61 · 10 ⁻¹⁸	0.75	Sander et al. (2011)

Table A5Photolysis rates for the 200 nm experiment. Photon flux is determined by fitting the N₂O concentration to the experimental values.

photolysis rate/s ⁻¹	reaction
1.11 · 10 ⁻⁷	N ₂ O → O(¹ D) + N ₂
8.84 · 10 ⁻⁷	NO ₂ → NO + O(¹ D)
7.84 · 10 ⁻⁶	NO ₃ → NO ₂ + O(¹ D)
9.22 · 10 ⁻⁷	O ₃ → O(¹ D) + O ₂
2.62 · 10 ⁻⁵	N ₂ O ₅ → NO ₃ + NO + O(³ P)
2.09 · 10 ⁻¹⁰	O ₂ → 2O(³ P)
1.06 · 10 ⁻⁵	HO ₂ → O(¹ D) + OH
2.59 · 10 ⁻⁹	H ₂ O → OH + H
1.37 · 10 ⁻⁶	H ₂ O ₂ → 2 OH
6.05 · 10 ⁻⁶	HONO → H + NO ₂
5.65 · 10 ⁻⁶	HNO ₃ → OH + NO ₂
1.13 · 10 ⁻⁵	HNO ₃ → HONO + O(¹ D)
4.06 · 10 ⁻⁶	HO ₂ NO ₂ → OH + NO ₃
1.22 · 10 ⁻⁵	HO ₂ NO ₂ → HO ₂ + NO ₂

Table A6

Photolysis rates for the 214 nm experiment. Photon flux is determined by fitting the N₂O concentration to the experimental values.

photolysis rate/s ⁻¹	reaction
$1.56 \cdot 10^{-8}$	N ₂ O → O(¹ D) + N ₂
$1.89 \cdot 10^{-7}$	NO ₂ → NO + O(¹ D)
$1.38 \cdot 10^{-7}$	NO ₃ → NO ₂ + O(¹ D)
$3.68 \cdot 10^{-7}$	O ₃ → O(¹ D) + O ₂
$1.31 \cdot 10^{-6}$	N ₂ O ₅ → NO ₃ + NO + O(³ P)
$2.33 \cdot 10^{-11}$	O ₂ → 2O(³ P)
$1.57 \cdot 10^{-6}$	HO ₂ → O(¹ D) + OH
$1.25 \cdot 10^{-7}$	H ₂ O ₂ → 2 OH
$7.86 \cdot 10^{-7}$	HONO → H + NO ₂
$5.96 \cdot 10^{-8}$	HNO ₃ → OH + NO ₂
$1.19 \cdot 10^{-7}$	HNO ₃ → HONO + O(¹ D)
$1.64 \cdot 10^{-7}$	HO ₂ NO ₂ → OH + NO ₃
$4.92 \cdot 10^{-7}$	HO ₂ NO ₂ → HO ₂ + NO ₂

Table A7

Wall-loss reactions included in the model, van der Waals radii of the species, and wall-loss rates. Wall loss of N₂O is estimated from the blank experiment, while the other reactions are calculated as diffusion of a two-component system with N₂ as the only bath gas.

species	radius/10 ⁻¹⁰ m	wall-loss rate/s ⁻¹
N ₂ O → wall·N ₂ O		$2.5 \cdot 10^{-9}$
N ₂ → wall·N ₂	2.18	0
O(³ P) → wall·O(P)	1.47	0.253495
NO → wall·NO	2.26	0.210422
NO ₂ → wall·NO ₂	4.14	0.168435
NO ₃ → wall·NO ₃	4.72	0.157105
HNO ₃ → wall·HNO ₃	4.95	0.154357
HO ₂ NO ₂ → wall·HO ₂ NO ₂	5.97	0.142066
HONO → wall·HONO	4.87	0.159151
OH → wall·OH	1.92	0.236884
H → wall·H	1.2	0.473705
H ₂ O ₂ → wall·H ₂ O ₂	4.59	0.179288
HO ₂ → wall·HO ₂	3.8	0.214067
N ₂ O ₅ → wall·N ₂ O ₅	6.21	0.137486

Table A8

Sampling loss for the 200 nm experiment. The sampling loss is determined from exponential fit to the starting and final pressure in the photoreactor.

sampling loss/s ⁻¹	reaction
$7.08 \cdot 10^{-7}$	O ₃ → loss
$7.08 \cdot 10^{-7}$	O(¹ D) → loss
$7.08 \cdot 10^{-7}$	O ₂ → loss
$7.08 \cdot 10^{-7}$	O(³ P) → loss
$7.08 \cdot 10^{-7}$	N ₂ → loss
$7.08 \cdot 10^{-7}$	N ₂ O → loss
$7.08 \cdot 10^{-7}$	NO → loss
$7.08 \cdot 10^{-7}$	NO ₂ → loss
$7.08 \cdot 10^{-7}$	NO ₃ → loss
$7.08 \cdot 10^{-7}$	N ₂ O ₅ → loss
$7.08 \cdot 10^{-7}$	H → loss
$7.08 \cdot 10^{-7}$	OH → loss
$7.08 \cdot 10^{-7}$	HO ₂ → loss
$7.08 \cdot 10^{-7}$	H ₂ O ₂ → loss
$7.08 \cdot 10^{-7}$	H ₂ O → loss
$7.08 \cdot 10^{-7}$	HNO ₃ → loss
$7.08 \cdot 10^{-7}$	HONO → loss
$7.08 \cdot 10^{-7}$	HO ₂ NO ₂ → loss

Table A9

Sampling loss for the 214 nm experiment. The sampling loss is determined from exponential fit, to the starting and final pressure in the photoreactor.

sampling loss/s ⁻¹	reaction
$3.14 \cdot 10^{-7}$	O ₃ → loss
$3.14 \cdot 10^{-7}$	O(¹ D) → loss
$3.14 \cdot 10^{-7}$	O ₂ → loss
$3.14 \cdot 10^{-7}$	O(³ P) → loss
$3.14 \cdot 10^{-7}$	N ₂ → loss
$3.14 \cdot 10^{-7}$	N ₂ → loss
$3.14 \cdot 10^{-7}$	NO → loss
$3.14 \cdot 10^{-7}$	NO ₂ → loss
$3.14 \cdot 10^{-7}$	NO ₃ → loss
$3.14 \cdot 10^{-7}$	N ₂ O ₅ → loss
$3.14 \cdot 10^{-7}$	H → loss
$3.14 \cdot 10^{-7}$	OH → loss
$3.14 \cdot 10^{-7}$	HO ₂ → loss
$3.14 \cdot 10^{-7}$	H ₂ O ₂ → loss
$3.14 \cdot 10^{-7}$	H ₂ O → loss
$3.14 \cdot 10^{-7}$	HNO ₃ → loss
$3.14 \cdot 10^{-7}$	HONO → loss
$3.14 \cdot 10^{-7}$	HO ₂ NO ₂ → loss

Table A10

Sensitivity analysis; f is the fraction of N₂O which reacts by photolysis

sensitivity analysis	f (200 nm)	error estimate (200 nm)/%	f (214 nm)	error estimate (214 nm)/%
standard model (10 $\mu\text{mol mol}^{-1}$ H ₂ O)	0.91757		0.78164	
photolysis 110%	0.91924	0.173	0.78925	0.974
photolysis 90%	0.91569	-0.214	0.77223	-1.204
pressure 110%	0.91759	-0.007	0.7811	-0.069
pressure 90%	0.91772	0.008	0.78226	0.079
radical loss x10	0.91768	0.003	0.78368	0.261
no radical loss	0.91746	-0.021	0.7865	0.622
100 $\mu\text{mol mol}^{-1}$ H ₂ O	0.91802	0.040	0.78299	0.173
1 $\mu\text{mol mol}^{-1}$ H ₂ O	0.91762	-0.003	0.7815	-0.018
no H ₂ O	0.91761	-0.004	0.78148	-0.020

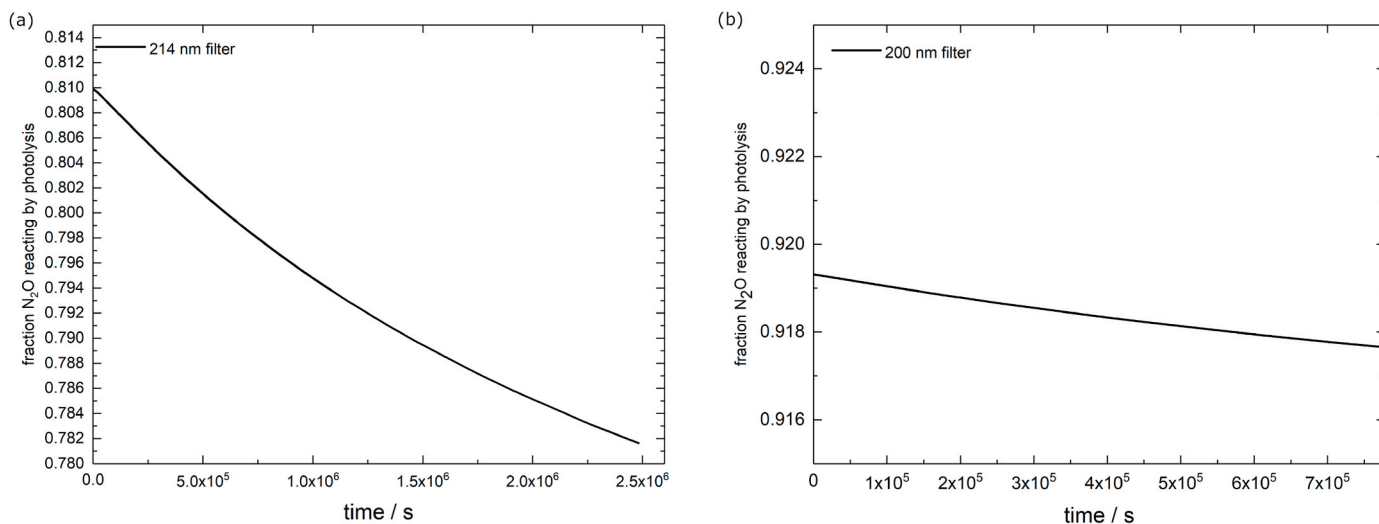


Fig. A1. Fraction of N₂O removed by photolysis in the experiments with (a) the 214 nm filter, (b) the 200 nm filter. The results are obtained from the box model.

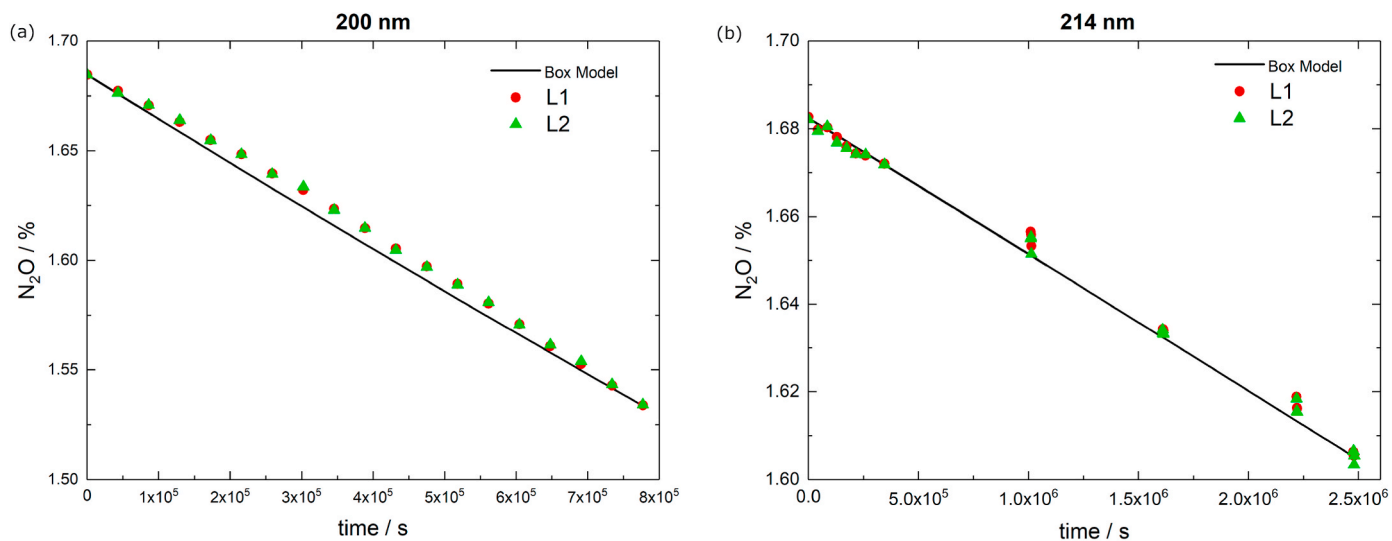


Fig. A2. N_2O concentration measured in the experiment and modeled by the box model in the experiment with (a) the 200 nm filter, (b) the 214 nm filter. L1, L2 indicates species 446 measured by laser 1 and laser 2, respectively.

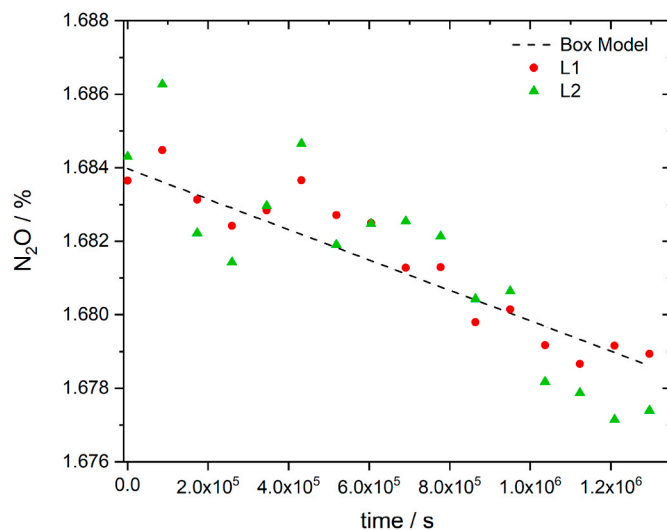


Fig. A3. N_2O concentration in the blank experiment (species 446 measured by laser 1 (L1) and laser 2 (L2)), and the N_2O concentration from the box model.

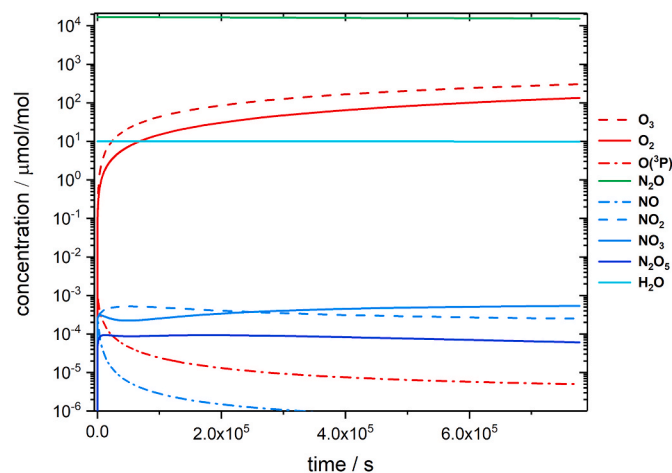


Fig. A4. Temporal evolution of N_2O (educt) and the most abundant product species in the box model for the 200 nm experiment.

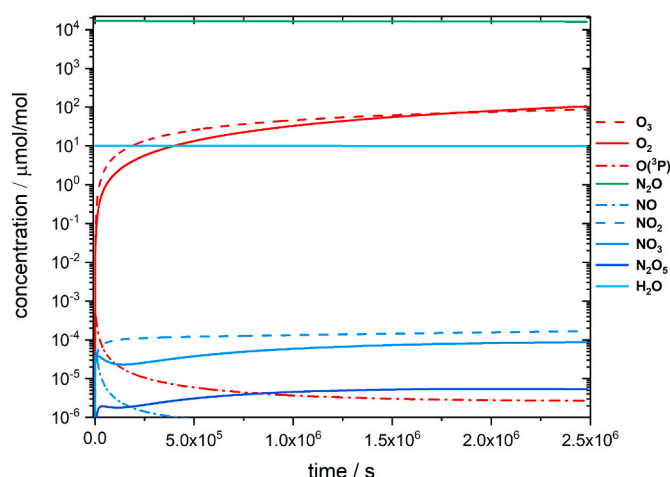


Fig. A5. Temporal evolution of N_2O (educt) and the most abundant product species in the box model for the 214 nm experiment.

References

- Bass, A.M., Ledford Jr., A.E., Laufer, A.H., 1976. Extinction coefficients of NO_2 and N_2O_4 . *J. Res. Natl. Bur. Stand., Sect. A* 80, 143. <https://doi.org/10.6028/jres.080A.017>.
- Eiler, J.M., 2007. Clumped-isotope geochemistry-The study of naturally-occurring, multiply-substituted isotopologues. *Earth Planet Sci. Lett.* 262, 309–327. <https://doi.org/10.1016/j.epsl.2007.08.020>.
- Griffis, T.J., Chen, Z., Baker, J.M., Wood, J.D., Millet, D.B., Lee, X., Venterea, R.T., Turner, P.A., 2017. Nitrous oxide emissions are enhanced in a warmer and wetter world. *Proc. Natl. Acad. Sci. U.S.A.* 114, 12081–12085. <https://doi.org/10.1073/pnas.1704552114>.
- Johnson, M.S., Billing, G.D., Gruodis, A., Janssen, M.H., 2001. Photolysis of nitrous oxide isotopomers studied by time-dependent hermite propagation. *J. Phys. Chem.* 105, 8672–8680. <https://doi.org/10.1021/jp011449x>.
- Johnston, J.C., Cliff, S.S., Thiemens, M.H., 1995. Measurement of multioxygen isotopic ($\delta^{18}\text{O}$ and $\delta^{17}\text{O}$) fractionation factors in the stratospheric sink reactions of nitrous oxide. *J. Geophys. Res. Atmos.* 100, 16801–16804. <https://doi.org/10.1029/95JD01646>.
- Kaiser, J., Brenninkmeijer, C.A., Röckmann, T., 2002a. Intramolecular ^{15}N and ^{18}O fractionation in the reaction of N_2O with $\text{O}(^1\text{D})$ and its implications for the stratospheric N_2O isotope signature. *J. Geophys. Res. Atmos.* 107 <https://doi.org/10.1029/2001JD001506>. ACH-16.
- Kaiser, J., Röckmann, T., Brenninkmeijer, C.A.M., 2004. Contribution of mass-dependent fractionation to the oxygen isotope anomaly of atmospheric nitrous oxide. *J. Geophys. Res. Atmos.* 109 <https://doi.org/10.1029/2003JD004088>.
- Kaiser, J., Röckmann, T., Brenninkmeijer, C.A., 2002b. Temperature dependence of isotope fractionation in N_2O photolysis. *Phys. Chem. Chem. Phys.* 4, 4420–4430. <https://doi.org/10.1039/B204837j>.
- Kaiser, J., Röckmann, T., Brenninkmeijer, C.A.M., 2003a. Assessment of $^{15}\text{N}^{15}\text{N}^{16}\text{O}$ as a tracer of stratospheric processes. *Geophys. Res. Lett.* 30, 16–19. <https://doi.org/10.1029/2002GL016253>.
- Kaiser, J., Röckmann, T., Brenninkmeijer, C.A.M., Crutzen, P.J., 2003b. Wavelength dependence of isotope fractionation in N_2O photolysis. *Atmos. Chem. Phys.* 3, 303–313. <https://doi.org/10.5194/acp-3-303-2003>.
- Kantnerová, K., Tuzson, B., Emmenegger, L., Bernasconi, S., Mohn, J., 2019. Quantifying isotopic signatures of N_2O using quantum cascade laser absorption spectroscopy. *Chimia* 73, 232–238. <https://doi.org/10.2533/chimia.2019.232>.
- Kantnerová, K., Yu, L., Zindel, D., Zahniser, M.S., Nelson, D.D., Tuzson, B., Nakagawa, M., Toyoda, S., Yoshida, N., Emmenegger, L., Bernasconi, S.M., Mohn, J., 2020. First investigation and absolute calibration of clumped isotopes in N_2O by mid-IR laser spectroscopy. *Rapid Commun. Mass Spectrom.* 34. <https://doi.org/10.1002/rcm.8836>.
- Kim, K.R., Craig, H., 1993. Nitrogen-15 and oxygen-18 characteristics of nitrous oxide: a global perspective. *Science* 262, 1855–1857. <https://doi.org/10.1126/science.262.5141.1855>.
- Magyar, P.M., Orphan, V.J., Eiler, J.M., 2016. Measurement of rare isotopologues of nitrous oxide by high-resolution multi-collector mass spectrometry. *Rapid Commun. Mass Spectrom.* 30, 1923–1940. <https://doi.org/10.1002/rcm.7671>.
- Minschwaner, K., Salawitch, R.J., McElroy, M.B., 1993. Absorption of solar radiation by O_2 : implications for O_3 and lifetimes of N_2O , CFCl_3 , and CF_2Cl_2 . *J. Geophys. Res. Atmos.* 98, 10543–10561. <https://doi.org/10.1029/93JD00223>.
- Moore, H., 1974. Isotopic measurement of atmospheric nitrogen compounds. *Tellus* 26, 169–174. <https://doi.org/10.1111/j.2153-3490.1974.tb01963.x>.
- Nambu, S., Johnson, M.S., 2004. Analysis of the ultraviolet absorption cross sections of six isotopically substituted nitrous oxide species using 3D wave packet propagation. *J. Phys. Chem.* 108, 8905–8913. <https://doi.org/10.1021/jp048853r>.
- Ostrom, N.E., Ostrom, P.H., 2017. Mining the isotopic complexity of nitrous oxide: a review of challenges and opportunities. *Biogeochemistry* 132, 359–372. <https://doi.org/10.1007/s10533-017-0301-5>.
- Peterson, B., Fry, B., 1987. Stable isotopes in ecosystem studies. *Annu. Rev. Ecol. Systemat.* 18, 293–320. <https://doi.org/10.1146/annurev.es.18.110187.001453>.
- Rahn, T., Wahlen, M., 1997. Stable isotope enrichment in stratospheric nitrous oxide. *Science* 278, 1776–1778. <https://doi.org/10.1126/science.278.5344.1776>.
- Ravishankara, A., Daniel, J.S., Portmann, R.W., 2009. Nitrous oxide (N_2O): the dominant ozone-depleting substance emitted in the 21st century. *Science* 326, 123–125. <https://doi.org/10.1126/science.1176985>.
- Röckmann, T., Brenninkmeijer, C.A., Wollenhaupt, M., Crowley, J.N., Crutzen, P.J., 2000. Measurement of the isotopic fractionation of $^{15}\text{N}^{14}\text{N}^{16}\text{O}$, $^{14}\text{N}^{15}\text{N}^{16}\text{O}$ and $^{14}\text{N}^{14}\text{N}^{18}\text{O}$ in the UV photolysis of nitrous oxide. *Geophys. Res. Lett.* 27, 1399–1402. <https://doi.org/10.1029/1999GL011135>.
- Röckmann, T., Kaiser, J., Brenninkmeijer, C.A., Crowley, J.N., Borchers, R., Brand, W.A., Crutzen, P.J., 2001. Isotopic enrichment of nitrous oxide ($^{15}\text{N}^{14}\text{N}^{16}\text{O}$, $^{14}\text{N}^{15}\text{N}^{16}\text{O}$, $^{14}\text{N}^{14}\text{N}^{18}\text{O}$) in the stratosphere and in the laboratory. *J. Geophys. Res. Atmos.* 106, 10403–10410. <https://doi.org/10.1029/2000JD900822>.
- Rothman, L., Gordon, I., Babikov, Y., Barbe, A., Chris Benner, D., Bernath, P., Birk, M., Bizzocchi, L., Boudon, V., Brown, L., Campargue, A., Chance, K., Cohen, E., Coudert, L., Devi, V., Drouin, B., Fayt, A., Flaud, J.M., Gamache, R., Harrison, J., Hartmann, J.M., Hill, C., Hodges, J., Jacquemart, D., Jolly, A., Lamouroux, J., Le Roy, R., Li, G., Long, D., Lyulin, O., Mackie, C., Massie, S., Mikhailenko, S., Müller, H., Naumenko, O., Nikitin, A., Orphal, J., Perevalov, V., Perrin, A., Polovtseva, E., Richard, C., Smith, M., Starikova, E., Sung, K., Tashkun, S., Tennyson, J., Toon, G., Tyuterev, V., Wagner, G., 2013. The HITRAN2012 molecular spectroscopic database. *J. Quant. Spectrosc. Radiat. Transfer* 130, 4–50. <https://doi.org/10.1016/j.jqsrt.2013.07.002>.
- Sander, S.P., 1986. Temperature dependence of the nitrogen trioxide absorption spectrum. *J. Phys. Chem.* 90, 4135–4142. <https://doi.org/10.1021/j100408a060>.
- Sander, S.P., Abbatt, J., Barker, J.R., Burkholder, J.B., Friedl, R.R., Golden, D.M., Huie, R.E., Kolb, C.E., Kurylo, M.J., Moortgat, G.K., Orkin, V.L., Wine, P.H., 2011. Chemical kinetics and photochemical data for use in atmospheric studies, evaluation no. 17. <http://jpldataeval.jpl.nasa.gov>.
- Schmidt, J.A., Johnson, M.S., 2015. Clumped isotope perturbation in tropospheric nitrous oxide from stratospheric photolysis. *Geophys. Res. Lett.* 42, 3546–3552. <https://doi.org/10.1002/2015GL063102>.
- Schmidt, J.A., Johnson, M.S., Schinke, R., 2011. Isotope effects in N_2O photolysis from first principles. *Atmos. Chem. Phys.* 11, 8965. <https://doi.org/10.5194/acp-11-8965-2011>.
- Selwyn, G., Podolske, J., Johnston, H.S., 1977. Nitrous oxide ultraviolet absorption spectrum at stratospheric temperatures. *Geophys. Res. Lett.* 4, 427–430. <https://doi.org/10.1029/GL004i010p00427>.
- Syakila, A., Kroeze, C., 2011. The global nitrous oxide budget revisited. *Greenhouse Gas Meas. Manage.* 1, 17–26. <https://doi.org/10.3763/ghgmm.2010.0007>.
- Toyoda, S., Yoshida, N., 1999. Determination of nitrogen isotopomers of nitrous oxide on a modified isotope ratio mass spectrometer. *Anal. Chem.* 71, 4711–4718. <https://doi.org/10.1021/ac9904563>.
- Toyoda, S., Yoshida, N., Koba, K., 2017. Isotopocule analysis of biologically produced nitrous oxide in various environments. *Mass Spectrom. Rev.* 36, 135–160. <https://doi.org/10.1002/mas.21459>.
- Toyoda, S., Yoshida, N., Morimoto, S., Aoki, S., Nakazawa, T., Sugawara, S., Ishidoya, S., Uematsu, M., Inai, Y., Hasebe, F., Ikeda, C., Honda, H., Ishijima, K., 2018. Vertical distributions of N_2O isotopocules in the equatorial stratosphere. *Atmos. Chem. Phys.* 18, 833–844. <https://doi.org/10.5194/acp-18-833-2018>.

- Tsang, W., Hampson, R., 1986. Chemical kinetic data base for combustion chemistry. Part I. Methane and related compounds. *J. Phys. Chem. Ref. Data* 15. <https://doi.org/10.1063/1.555759>, 1087–1279.
- Turatti, F., Griffith, D., Wilson, S., Esler, M., Rahn, T., Zhang, H., Blake, G., 2000. Positionally dependent ^{15}N fractionation factors in the UV photolysis of N_2O determined by high resolution FTIR spectroscopy. *Geophys. Res. Lett.* 27, 2489–2492. <https://doi.org/10.1029/2000GL011371>.
- Umemoto, H., 1999. $^{14}\text{N}/^{15}\text{N}$ isotope effect in the UV photodissociation of N_2O . *Chem. Phys. Lett.* 314, 267–272. [https://doi.org/10.1016/S0009-2614\(99\)01145-8](https://doi.org/10.1016/S0009-2614(99)01145-8).
- Von Hessberg, P., Kaiser, J., Enghoff, M., McLinden, C.A., Sorensen, S., Röckmann, T., Johnson, M.S., 2004. Ultra-violet absorption cross sections of isotopically substituted nitrous oxide species: $^{14}\text{N}^{14}\text{NO}$, $^{15}\text{N}^{14}\text{NO}$, $^{14}\text{N}^{15}\text{NO}$ and $^{15}\text{N}^{15}\text{NO}$. *Atmos. Chem. Phys.* <https://doi.org/10.5194/acp-4-1237-2004>.
- World Meteorological Organization, Global Atmosphere Watch, 2019. WMO GREENHOUSE GAS BULLETIN.
- York, D., Evensen, N.M., Martínez, M.L., De Basabe Delgado, J., 2004. Unified equations for the slope, intercept, and standard errors of the best straight line. *Am. J. Phys.* 72, 367–375. <https://doi.org/10.1119/1.1632486>.
- Yu, L., Harris, E., Lewicka-Szczepak, D., Barthel, M., Blomberg, M.R., Harris, S.J., Johnson, M.S., Lehmann, M.F., Liisberg, J., Müller, C., Ostrom, N.E., Six, J., Toyoda, S., Yoshida, N., Mohn, J., 2020. What can we learn from N_2O isotope data? –Analytics, processes and modelling. *Rapid Commun. Mass Spectrom.* n/a. <https://doi.org/10.1002/rcm.8858>.
- Yung, Y.L., Miller, C.E., 1997. Isotopic fractionation of stratospheric nitrous oxide. *Science* 278, 1778–1780. <https://doi.org/10.1126/science.278.5344.1778>.
- Zhang, H., Wennberg, P.O., Wu, V.H., Blake, G.A., 2000. Fractionation of $^{14}\text{N}^{15}\text{N}^{16}\text{O}$ and $^{15}\text{N}^{14}\text{N}^{16}\text{O}$ during photolysis at 213 nm. *Geophys. Res. Lett.* 27, 2481–2484. <https://doi.org/10.1029/1999GL011236>.